Microporous and Mesoporous Materials 307 (2020) 110470

Contents lists available at ScienceDirect

Microporous and Mesoporous Materials

journal homepage: http://www.elsevier.com/locate/micromeso

The influence of intrapore cation on the fluorination of zeolite Y

Daniel S. Parsons [a,b,*], David C. Apperley [c], Andrew Ingram [d], Joseph A. Hriljac [a,b,**]

[a] School of Chemistry, University of Birmingham, Birmingham, B15 2TT, UK
[b] Diamond Light Source, Harwell Science and Innovation Campus, Didcot, OX11 0DE, UK
[c] Department of Chemistry, Durham University, Durham, DH1 3LE, UK
[d] School of Chemical Engineering, University of Birmingham, Birmingham, B15 2TT, UK

ARTICLE INFO

Keywords:
Zeolite
Fluoride
Fluorination
Defluoridation
Silanol

ABSTRACT

The influence of the intrapore cation on the fluorination of zeolite Y from dilute fluoride solutions has been studied, revealing fluoride reacts with the zeolite framework in the presence of a Brønsted acid to form [SiO_3F] and [AlO_3F] moieties. $^{29}Si\{^1H\}$ Cross-polarised MAS NMR indicates the reaction proceeds by the substitution of surface hydroxide moieties for fluoride. The fluorination reaction is strongly influenced by the nature of the intrapore cation. Intrapore Brønsted acids facilitate fluorination of the framework by *in situ* ion-exchange, releasing the acidic ions to the zeolite surface. The fluorination reaction may be further promoted by the presence of intrapore alkaline earth cations (viz. Mg^{2+}, Ca^{2+}, Sr^{2+} and Ba^{2+}). The conclusions of this work are significant to the preparation of fluorinated zeolite catalysts, the application of zeolites in defluoridation and the labelling of zeolite-based tracers with ^{18}F for application in positron imaging techniques.

1. Introduction

Fluoride may be used as a mineraliser to catalyse condensation reactions in sol-gel syntheses of zeolites and related materials. In many cases, fluoride ions remain in cages in the products [1–7] where they may also bond to silicon atoms forming five co-ordinate [SiO_4F] species [4–7]. Alternatively, fluoride may be incorporated into zeolites post-synthesis from aqueous solutions. Previous studies on fluoride uptake by zeolites from aqueous solutions can generally be divided into two categories: studies where zeolites are evaluated as adsorbents for aqueous fluoride removal [8–14], and studies where fluoride is reacted with the zeolite to modify the properties of the surface for catalytic applications [15–21].

Studies that evaluate zeolite efficacy in aqueous fluoride removal (defluoridation) are usually simple in conception, involving measuring the amount of fluoride removed from solution by a natural zeolite [8–10], or a zeolite modified with surface-sorbed trivalent cations [11–14], using a fluoride ion-selective electrode. Post-treatment characterisation of the zeolite is not reported in any case and mechanistic understanding is limited to information gleaned from fitting equilibrium uptake data to adsorption isotherms.

Defluoridation has been demonstrated for natural samples of clinoptilolite [8], analcime [8] and stilbite [8–10]. For stilbite, the Ca form (Ca-STI) achieves higher fluoride loadings than the Na form (Na-STI) [9]. In another study on Ca/NH_4-STI and Ca/Na-STI, fluoride uptake was attributed to "connectivity defects" and ion-exchange leading to CaF_2 precipitation, respectively [10]; however, neither conclusion is supported by any evidence. Hitherto, the mechanism by which fluoride interacts with zeolites in dilute solutions has been unknown and subject to supposition.

The modification of zeolites with Fe^{3+} (stilbite) [11], Al^{3+} (zeolites A, X, Y and clinoptilolite) [12–14] and La^{3+} (clinoptilolite) [13] has given rise to appreciable fluoride loadings. Fits to the Dubinin-Radushkevitch isotherm reveal fluoride interacts by chemisorption with Al^{3+}-modified zeolites A, X and Y [12,14]. In these modified zeolites, it is believed fluoride substitutes for a hydroxide in surface-sorbed M^{3+}-complexes [12,14].

In studies where zeolites are fluorinated to modify the properties of the surface for enhanced catalytic performance, the zeolite is typically treated with a concentrated acid solution containing NH_4F and heated under reflux or hydrothermal conditions for a period of hours to days [15–19]. Alternatively, the zeolite may be loaded with a fluoride containing solution by incipient wetness impregnation followed by thermal treatment at *ca.* 500 °C [20,21]. The zeolites are typically those of

* Corresponding author. Diamond Light Source, Harwell Science and Innovation Campus, Didcot, OX11 0DE, UK.
** Corresponding author. Diamond Light Source, Harwell Science and Innovation Campus, Didcot, OX11 0DE, UK.
E-mail addresses: daniel.parsons@diamond.ac.uk (D.S. Parsons), joseph.hriljac@diamond.ac.uk (J.A. Hriljac).

https://doi.org/10.1016/j.micromeso.2020.110470
Received 6 March 2020; Received in revised form 23 June 2020; Accepted 4 July 2020
Available online 25 July 2020

catalytic significance such as ZSM-5 or related materials such as titanosilicates with the MOR structure [16,20]. ^{19}F MAS NMR spectroscopy has confirmed the presence of [SiO_3F] [15–18], [SiO_4F] [15–18] and [AlO_3F] [19] moieties in fluorinated zeolites and related materials, among species such as hexafluorosilicate ions attesting framework destruction in some instances [15–17].

The mechanism by which the fluorination of zeolites occurs is ascribed either to the addition of H^+F^- ion pairs across T-O-T bonds, or alternately, the substitution of fluoride for hydroxide at surface silanol (Si–OH) or aluminol (Al–OH) moieties. Decreasing intensities associated with silanol hydroxyl stretches in IR spectra are put forward to support the latter mechanism (substitution at surface hydroxide moieties) [15,21]. The only evidence put forward for the former mechanism is based on adsorption measurements to determine surface acidity which appears inconclusive and far from compelling [20].

Naturally, a greater understanding of how defluoridation by zeolites occurs from low concentration fluoride solutions could inform strategies to enhance fluoride loadings. Such strategies could also be applied to enhance fluoride loadings attained by large zeolite particles labelled with $^{18}F^-$ for application as radiotracers in positron imaging techniques, such as PEPT (Positron Emission Particle Tracking) [22]. In this study, we have investigated the interaction between dilute fluoride solutions and zeolites, determining the influence the intrapore cation has on the affinity for fluoride, the fluoride containing moieties present in the products and the likely mechanism by which defluoridation occurs.

2. Experimental

2.1. Materials

NH_4-zeolite Y (NH_4–Y) was obtained from Alfa-Aesar (product 45863). Na–Y was obtained from Sigma-Aldrich (product 334448). H–Y was produced by calcination of NH_4–Y at 550 °C in air in a muffle furnace for 5 h.

$M_x(NH_4)_{1-2x}$-Y and M_xNa_{1-2x}-Y (M = Mg, Ca, Sr or Ba) species were prepared by ion-exchange of the parent materials, NH_4–Y and Na–Y, respectively, with 0.25 M solutions of the appropriate divalent metal nitrate salt agitated at 60 °C in a Memmert WNB14 shaking water bath for 24 h (zeolite to solution ratio of 0.5 g:50 ml). Divalent metal nitrate salts employed were $Mg(NO_3)_2.6H_2O$ (Sigma Aldrich, 99%), $Ca(NO_3)_2.4H_2O$ (Acros Organics, 99%), $Sr(NO_3)_2$ (Alfa Aesar, 99%) and $Ba(NO_3)_2$ (Sigma Aldrich, 99%). Following ion-exchange, the products were collected by vacuum filtration, washed copiously with deionised H_2O and dried overnight at 60 °C.

2.2. Batch fluoride adsorption measurements

Sodium fluoride solutions in the desired concentration range (5–60 ppm fluoride) were made by dilution of the appropriate volume of 1000 ppm fluoride (1 g L^{-1}) NaF solution (Hanna Instruments, HI70701L) with deionised water in polypropylene volumetric flasks. *Ca.* 0.100 g of zeolite, weighed accurately to 3 decimal places, was added to the solution (20 ml) of desired concentration in a polypropylene vessel (capacity = 60 ml, diameter = 28 mm). The vessels were placed in a Memmert WNB14 water bath equipped with a shaking attachment and shaken laterally at approx. 110 shakes per minute for 24 h, at the specified temperature. Following 24 h, 15 ml of supernatant solution was decanted and added to 3 ml of TISAB-II buffer (Hanna Instruments, HI401005L). The potential of the solution (mV) was measured with a calibrated fluoride ion-selective electrode (Cole Parmer) connected to a Hanna Instruments HI 3222 processor, calibrated across the range 1–100 ppm fluoride with standards (1, 10 and 100 ppm fluoride) made by serial dilution of 1000 ppm F^- NaF solution. Calibrants were also prepared in a 5:1 mixture with TISAB-II. Solution fluoride concentrations were calculated from the appropriate calibration curve. Calibrant and analyte solutions were stirred while measuring to ensure accurate readings. Blank measurements were employed for all analyte solutions of a given concentration to adjust for any adsorption to the vessel. Fluoride loadings (mg F^-/g) of the initial zeolite material were calculated by equation (1).

$$F^- \text{ loading } (\text{mg } F^-/\text{g}) = (c_0 - c_e)/\rho; \text{ where} \rho = m/v \quad (1)$$

In Equation (1), c_0 and c_e are the initial and equilibrium fluoride concentrations (mg L^{-1}), respectively, as measured by a calibrated fluoride ion-selective electrode (ISE). V is the volume of the solution (L) and m is the initial mass of the zeolite (g).

In solutions which were analysed by ICP-OES to determine the Na^+ concentration, solutions were made by dilution of 1000 ppm F^- (1 g L^{-1}) NaF solution (Hanna Instruments, HI70701L) with ultrapure water. Circa 0.150 g portions of zeolites H–Y or NH_4–Y, weighed accurately to 3 decimal places, were added to the NaF solutions (30 ml). The solutions were added to the water bath with shaking attachment at 25 °C as described earlier and shaken for 24 h. After 24 h, solutions were filtered through a 0.2 μm filter. Aliquots (15 ml) of the filtered solution were added to TISAB-II (3 ml); the fluoride concentration was then measured as described above. Separate aliquots of the filtered analyte solution (9.71 ml) were diluted and acidified by the addition of 0.29 ml of 67 wt % ultrapure HNO_3 (VWR, NORMATOM™) rendering the final analyte solution 2 wt% HNO_3.

1:1 NaF:HNO_3 solutions, in the range 5–60 ppm fluoride, were prepared by dilution of the appropriate amount of 1000 ppm F^- (1 g L^{-1}) NaF solution (Hanna Instruments, HI70701L) with deionised water, where the required amount of 0.1 M HNO_3 to render the final solution 1:1 NaF:HNO_3 was added during dilution (e.g. in producing 250 ml of a 1:1 NaF:HNO_3 solution with concentration 20 ppm F^-, 2.60 ml of 0.1 M HNO_3 was added during dilution). Batch adsorption experiments with Na–Y proceeded as described earlier with the 1:1 NaF:HNO_3 solutions.

2.3. Characterisation

Powder X-ray diffraction (PXRD) was performed on a Bruker D8 Advance diffractometer in reflection geometry equipped with a Ni-filtered Cu K_α X-ray source (λ = 1.5418 Å) and fitted with a solid-state LynxEye position sensitive detector. Scans were measured over the 2θ range 4–60° at a scan rate of 0.04° s^{-1} with a step-size of 0.02°.

XRF spectrometry was performed on a Bruker S8 Tiger spectrometer. All samples were measured as loose powders mounted on Mylar™ film for the maximum 18-min data collection time. Quantitative results were obtained from SPECTRA^{plus} software. The K_α emission line was used to quantify all elements, except for Sr and Ba which were instead quantified by the L_α emission line.

Scanning electron micrographs were obtained on a Phillips XL30 ESEM FEG microscope at an accelerating voltage of 20 keV and a working distance of 10 mm. The imaged samples were mounted on graphite tape then sputter coated with a gold thin film prior to imaging.

Solid-state ^{29}Si NMR spectra were acquired using a Varian VNMRS spectrometer operating at 79.44 MHz for silicon, with a 6 mm (rotor outside diameter) magic-angle spinning (MAS) probe and at a sample spin-rate of approximately 6 kHz. Direct excitation spectra were obtained following a 90° pulse with a 240 or 60 s recycle delay for H–Y and $Sr_{0.14}(NH_4)_{0.72}$-Y, respectively. Cross-polarisation spectra were recorded using a 10 ms contact time and 1 s recycle delay. Spectral referencing is with respect to tetramethylsilane, carried out by setting the high-frequency resonance from tetrakis(trimethylsilyl)silane to −9.9 ppm.

Fluorine-19 MAS NMR spectra were acquired using a Bruker Avance III HD spectrometer operating at 376.48 MHz for fluorine, with a 3.2 mm MAS probe and at a sample spin-rate of either 18 or 20 kHz. Spectra were acquired using a rotor-synchronised Hahn-echo and with a recycle delay of 4 s. Spectral referencing is with respect to $CFCl_3$, carried out by setting the resonance from a 50:50% v/v mixture of CF_3COOH/H_2O to −76.54 ppm. All MAS NMR spectra were recorded at ambient probe temperature.

ICP-OES analysis of Na concentrations was performed on a PerkinElmer OES Optima 8000 spectrometer. Calibrants, with concentrations 0.1, 1, 5, 10 and 100 ppm, were made by dilution of 1000 ppm Na standard solution (Centripur®) with ultrapure water. 67 wt% ultrapure HNO_3 (0.29 ml) was added to each calibrant solution (9.71 ml), such that each calibrant was acidified to *ca.* 2 wt% and to the same extent as the analyte solutions. A representative blank solution of ultrapure water (9.71 ml) was also acidified by addition of 67 wt% ultrapure HNO_3 (0.29 ml).

2.4. Adsorption isotherms

The Dubinin-Radushkevitch (DR) isotherm equation and its linear form, as commonly applied to adsorption at the solid-liquid interface, are presented in Equation (2). The adsorption potential (ε) in the DR isotherm may be calculated by Equation (3) [23,24]. The adsorbate solubility (c_s) used in Equation (3) was calculated at each temperature, using the equation presented in Reynolds and Belsher [25], then converted to ppm F^- ($c_s = 18803$ ppm F^- at 25 °C, and $c_s = 19621$ ppm F^- at 40 °C). The characteristic adsorption energy (E_c) may be derived from the Dubinin-Radushkevitch constant (K) by the relationship in Equation (4). Linear regression analysis to determine R^2, the gradient and y-intercept for each plot was performed in Sigmaplot software.

$$\ln q_e = \ln\left(\frac{V_O}{V_m}\right) - K\varepsilon^2 \quad (2)$$

Definitions for equation (2): q_e, equilibrium uptake (mg g^{-1}); K, Dubinin-Radushkevitch constant (mol^2 kJ^{-2}); ε, adsorption potential (kJ mol^{-1}); V_O, specific micropore volume (cm^3 g^{-1}); V_m, volume of the adsorbate (cm^3 mg^{-1}).

$$\varepsilon = RT \ln\left(\frac{C_s}{C_e}\right) \quad (3)$$

Definitions for equation (3): R, universal gas constant (kJ K^{-1} mol^{-1}); T, absolute temperature (K); c_s, adsorbate solubility (mg L^{-1}).

$$E_c = (2K)^{-0.5} \quad (4)$$

Fits to the Langmuir, Temkin and Freundlich isotherms have also been tested and these isotherms, as well as plots and the results of fits (R^2 and isotherm parameters), may be found in the Supporting Information.

3. Results and discussion

3.1. H–Y, NH_4–Y and Na–Y: characterisation

The phase purities of H–Y, NH_4–Y and Na–Y were confirmed by PXRD (Supporting Information, Fig. S1). Unit cell parameters determined from a unit cell refinement by chekcell software [26] are also presented in the Supporting Information (Table S1). XRF spectrometry confirmed the Si/Al ratios of NH_4–Y (2.8(1)) and Na–Y (2.7(1)) are equivalent within error. The bulk Si/Al ratio of H–Y (2.7(1)) is within error of the parent material NH_4–Y (2.8(1)); however, intrapore aluminium-containing species are known to form during the calcination of NH_4–Y [27]. The framework Si/Al ratio of H–Y determined from deconvoluted integrals in the ^{29}Si MAS NMR spectrum is 4.7, attesting dealumination of the framework and the formation of intrapore aluminium-containing species. The ^{29}Si MAS NMR spectrum recorded on H–Y along with peak positions, assignments and integrals may be found in the Supporting Information (Fig. S2 and Table S2). Scanning electron micrographs of NH_4–Y, Na–Y and H–Y confirm a similar particle dispersity in each sample, generally spanning 0.3–2.0 μm for discrete particles with some larger aggregates also present (Supporting Information, Fig. S3).

3.2. H–Y, NH_4–Y and Na–Y: fluoride loadings

Equilibrium fluoride loadings from dilute NaF solutions (5–60 ppm F^-) achieved by the zeolites H–Y, NH_4–Y and Na–Y under isothermal conditions as measured by a fluoride ion-selective electrode (ISE) are plotted in Fig. 1 as a function of the initial fluoride concentration. The contact time for all solutions with the zeolite was 24 h, loadings measured following 48 and 72 h for H–Y show negligible variation from those measured after 24 h, indicating that equilibrium is achieved by 24 h of contact between the zeolite and solution. Changing the intrapore cation gives rise to markedly different equilibrium fluoride loadings across the concentration range. No detectable change in fluoride concentration occurs following contact with Na–Y, indicating negligible fluoride adsorption on this zeolite. In contrast, fluoride uptake is observed for both H–Y and NH_4–Y across the same concentration range under the same conditions. The fluoride loadings achieved by H–Y are greater than NH_4–Y from solutions with the same concentration; moreover, loadings for both zeolites increase upon increasing the temperature from 25 °C to 40 °C.

3.3. Role of Brønsted acids

While substantial fluoride uptake is observed for H–Y and NH_4–Y, negligible uptake under the same conditions is observed for Na–Y. The NH_4–Y and Na–Y employed possess similar particle sizes and bulk Si/Al ratios; the only obvious characteristic difference between the two zeolites is the nature of the intrapore cation. Unlike Na–Y, the intrapore cations in NH_4–Y and H–Y are Brønsted acids; it would appear these acidic cations are critical to the interaction occurring between the zeolite and aqueous fluoride.

Measurement of the Na^+ concentrations in supernatant solutions by ICP-OES, following 24 h of contact with the zeolite, confirms ion-exchange occurs between aqueous Na^+ ions and intrapore NH_4^+ or H^+ ions, in the case of NH_4–Y and H–Y, respectively. Fig. 2 presents a plot of equilibrium ion loading (mol g^{-1}), for both F^- and Na^+, for each zeolite at 25 °C as a function of initial fluoride concentration (ppm F^-), where F^- and Na^+ concentrations were determined by a F^- ISE and ICP-OES,

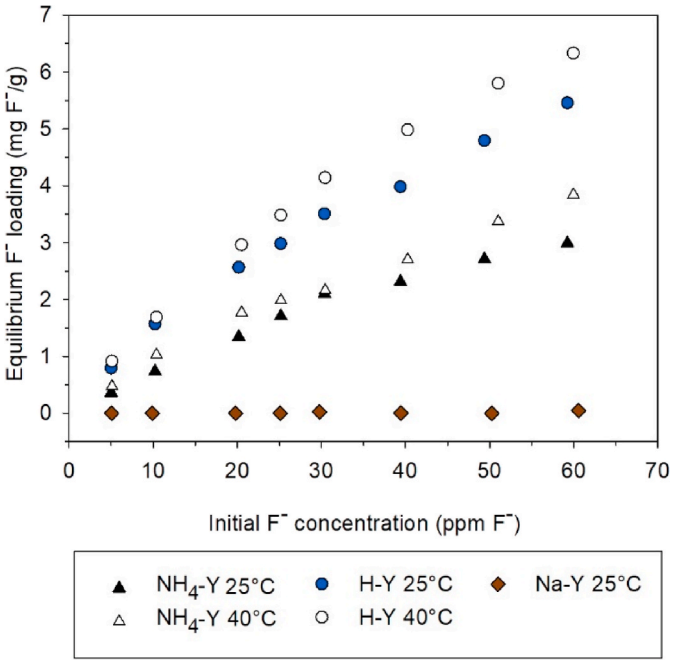

Fig. 1. A plot of equilibrium fluoride loading (mg F^-/g), by zeolites H–Y, NH_4–Y and Na–Y, at different temperatures as a function of initial fluoride concentration (ppm F^-).

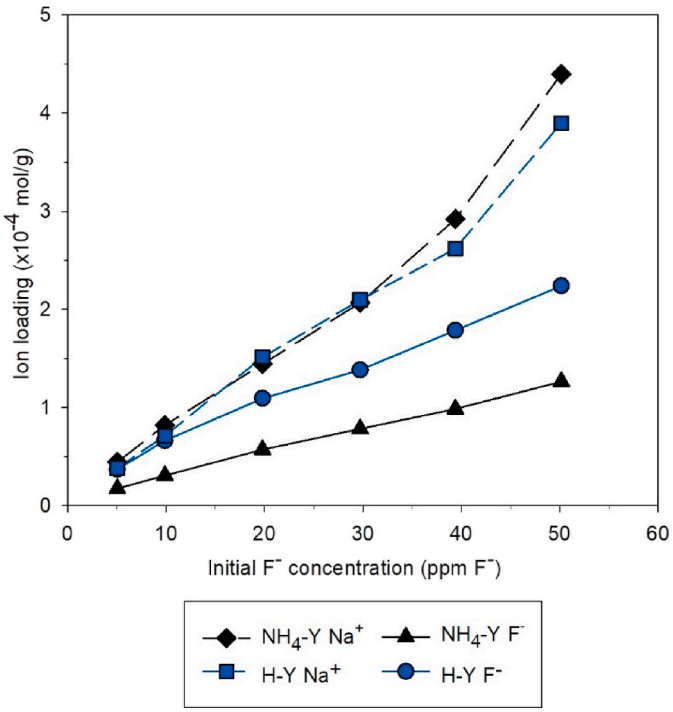

Fig. 2. Plot of Na^+ and F^- equilibrium ion loadings achieved for H–Y and NH_4–Y at 25 °C.

respectively, of the same supernatant solutions. In Fig. 2 lines join the data points to add clarity in areas where they are proximal. Fig. 2 shows that at each concentration for each zeolite, a higher Na^+ concentration is exchanged into the zeolite than the F^- concentration that is adsorbed to it, hence the concentration of H^+ or NH_4^+ ions released by ion-exchange is greater than the amount of F^- adsorbed. Consequently, a stoichiometric equivalence of H^+ or NH_4^+ ions migrate to the surface, where they may participate in fluoride adsorption.

XRF spectrometry performed on the zeolites, NH_4–Y and H–Y, following treatment with 60 ppm F^- NaF solutions at 25 °C and 40 °C for 24 h further attests that ion exchange occurs between the aqueous Na^+ ions and intrapore NH_4^+ or H^+ ions. A Na/Al ratio of 0.11(2) was measured for fluorinated H–Y samples treated at both 25 °C and 40 °C. Slightly higher Na/Al ratios of Na/Al = 0.13(2) and Na/Al = 0.14(2) were measured for NH_4–Y treated at 25 °C and 40 °C, respectively. Moreover, the Si/Al ratios measured for each fluorinated zeolite, at each temperature, agree with the Si/Al ratios measured for the parent materials within error. A Si/Al ratio of 2.7(1) was measured for each NH_4–Y and H–Y species fluorinated at either 25 °C or 40 °C. While treating zeolites with aqueous fluoride under driving conditions can often lead to dealumination [28], XRF analysis indicates there is no discernible dealumination occurring under the mild conditions employed in this study.

The pH of the NaF solutions are near neutral ranging from pH = 6.9 at 5 ppm F^-, decreasing slightly to pH = 6.7 at 60 ppm F^-. Consequently, the free [H^+] concentration in solution is negligible compared with the aqueous [F^-] concentration. The only source of protons to participate in adsorption are Brønsted acidic intrapore cations released following ion-exchange with Na^+. The essential role of a proton source in fluoride adsorption on the zeolites has been further confirmed by measuring fluoride loadings for Na–Y from fluoride solutions containing an equivalent source of protons. The fluoride loadings achieved by Na–Y from 1:1 NaF:HNO_3 solutions and pure NaF solutions are plotted in Fig. 3. Appreciable fluoride loadings are achieved by Na–Y when an equivalent source of H^+ is present in solution, whereas no fluoride is adsorbed from pure NaF solutions at near neutral pH, further supporting

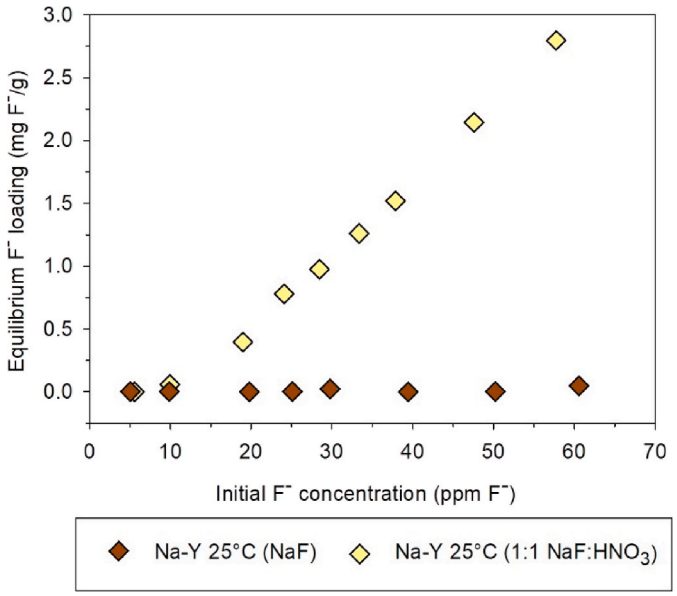

Fig. 3. Equilibrium fluoride loadings attained by Na–Y from NaF solutions (brown) and 1:1: NaF: HNO_3 solutions (yellow) as a function of initial F^- concentration. (For interpretation of the references to colour in this figure legend, the reader is referred to the Web version of this article.)

the essential role of H^+ in fluoride adsorption by zeolites.

The influence of protons on fluoride uptake has been further demonstrated by measuring fluoride loadings from acidic solutions. The pH of 60 ppm F^- NaF solutions were reduced to 4.1, 3.5 and 3.0 by the addition of 0.1 M HNO_3; fluoride loadings attained by Na–Y, H–Y and NH_4–Y at 25 °C from these solutions were measured and the results are plotted in Fig. S5 in the Supporting Information. A moderate increase in fluoride loading is observed for all zeolites upon lowering the pH from 6.7 to 4.1, with a further increase in loading upon reducing the pH to 3.5. In the case of NH_4–Y and Na–Y, a yet higher fluoride loading may be achieved at pH = 3.0; however, the fluoride loading attained for H–Y decreases upon lowering the pH from 3.5 to 3.0. Critically, fluoride uptake is observed for Na–Y in acidic media but not in near neutral solutions (pH = 6.7), further supporting the essential role of Brønsted acids in the fluorination of the zeolites.

3.4. H–Y and NH_4–Y: Dubinin-Radushkevitch (DR) isotherm

Good fits are observed to the linear DR equation for both zeolites at both temperatures, with $R^2 > 0.988$ in each case (plots presented in Fig. 4, and R^2 values and E_c values from the fits listed in Table 1). The DR isotherm is arguably the most informative model commonly applied to solid-liquid adsorption as it permits the determination of the characteristic adsorption energy (E_c), also termed the free energy of sorption, providing good fits are observed. The magnitude of E_c is indicative of the strength, and nature, of adsorption occurring; in instances where $E_c < 8$ kJ mol^{-1}, adsorption is attributed to physical adsorption, whereas values in the range $8 < E_c < 16$ kJ mol^{-1} are often ascribed to chemical adsorption [14]. The values of E_c calculated from the gradient (K) by the relationship, $E_c = 2K^{-0.5}$, are presented in Table 1. The magnitude of E_c for H–Y, at both 25 and 40 °C, indicates chemisorption is the dominant mode of adsorption taking place, intimating a chemical bond is being formed between fluoride and the zeolite.

The free energy of sorption, E_c, for NH_4–Y at 40 °C (8.5 kJ mol^{-1}) indicates chemisorption is taking place; however, at 25 °C the value of E_c for NH_4–Y (7.5 kJ mol^{-1}) falls below 8 kJ mol^{-1}, which by convention demarcates physical and chemical adsorption. Although the magnitude of E_c indicates fluoride interacts by physisorption to NH_4–Y at 25 °C, solid state NMR of NH_4–Y fluorinated at 25 °C, detailed later in Section

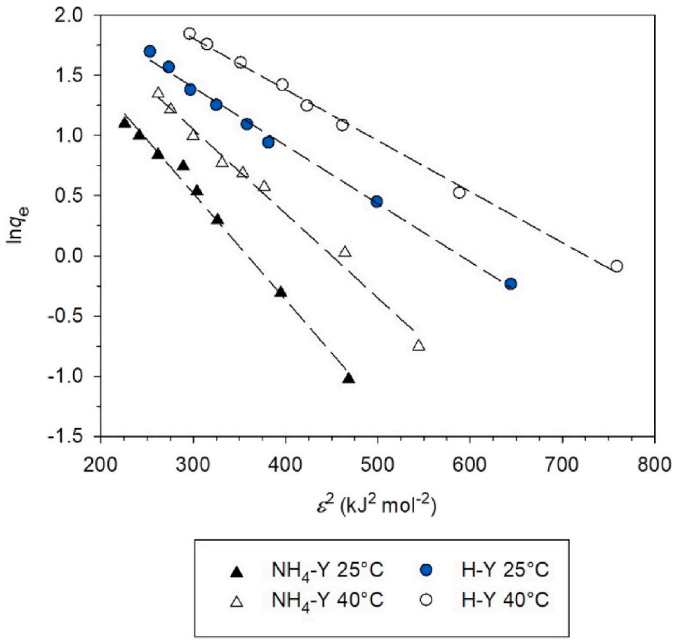

Fig. 4. Plot of adsorption data fitted to the linear DR equation for H–Y and NH_4–Y.

Table 1
Characteristic sorption energies (E_c) and R^2 for DR plots of H–Y and NH_4–Y.

Zeolite	T (°C)	R^2	E_c (kJ mol^{-1})
H–Y	25	0.995	10.2
	40	0.997	10.9
NH_4–Y	25	0.992	7.5
	40	0.989	8.5

3.5, shows fluoride reacts with, and forms a chemical bond to, the zeolite framework. Ultimately, the 8 kJ mol^{-1} value should be viewed as a guideline and the value of E_c at 25 °C reflects the lower favorability of the reaction at lower temperatures, rather than a weaker interaction with the adsorbent. The less favourable E_c values observed for NH_4–Y, compared with H–Y, may be because dissociation of the ammonium ion must occur to provide the proton which mediates the fluorination reaction.

3.5. H–Y and NH_4–Y: fluorine environments

Fluorine-19 MAS NMR spectra measured on H–Y and NH_4–Y, fluorinated by contact with 200 ppm F^- NaF solutions for 24 h at 25 °C, are presented in Fig. 5. Fluoride loadings of 29 and 20 mg F^-/g were measured for H–Y and NH_4–Y, respectively, by a fluoride ISE calibrated across the range 1–1000 ppm F^-. The H–Y and NH_4–Y fluorinated under these conditions will hereon be referred to as H–Y(F) and NH_4–Y(F). The ^{19}F MAS NMR spectra for H–Y(F) and NH_4–Y(F) contain 3 distinct resonances at approximately −119, −153 and −176 ppm. Recording the spectrum for H–Y(F) at different spin rates, 20 and 18 kHz, enabled centrebands to be differentiated from spinning sidebands. All the intensity outside the range −115 to −180 ppm is produced by spinning sidebands (denoted by asterisks in Fig. 5).

In the ^{19}F MAS NMR spectra, peak **B** at −153 ppm occurs at a chemical shift commonly associated with [SiO_3F] moieties in zeolites and other silicates [15–18,29,30]. Peak **B** has an asymmetric profile in both spectra. Peak fitting indicates there may be an additional resonance at $\delta_F \approx -135$ ppm in both spectra (Supporting Information), however this does not account for all the observed peak asymmetry. The possible origin of an additional resonance at $\delta_F \approx -135$ ppm is covered later (Section 3.9). The asymmetric profile may be indicative of multiple signals in the region giving rise to one unresolved peak. Several signals resulting from [SiO_3F] moieties could be expected in the ^{19}F MAS NMR spectra on account of the 4 observed silicon environments in the ^{29}Si MAS NMR spectra of both H–Y (Supporting Information) and NH_4–Y (Section 3.6).

Peak **C** at $\delta_F \approx -176$ ppm corresponds to those observed in a previous study on H–Y fluorinated by incipient wetness impregnation followed by high temperature treatment. ^{27}Al NMR experiments, including 2D NMR, in the study demonstrated the resonance was produced by fluorine atoms bonded to 4 co-ordinate aluminium atoms, i.e. [AlO_3F] [19].

Peak **A** at $\delta_F \approx -119$ ppm occurs at a chemical shift often associated with fluoride ions within the zeolite pores, but not within a cage, and charge compensated by an intrapore cation [19,28,31,32]. In ^{19}F NMR spectra, aqueous fluoride ions in sodium fluoride solutions produce a resonance at $\delta_F \approx -122$ ppm [33], similar to the chemical shift observed for intrapore fluoride within zeolites. As the anticipated environment of both would comprise hydrated fluoride ions, the similar chemical shifts are unsurprising. The charge on each intrapore fluoride ion must be compensated by an additional intrapore cation, the associated cation would be expected to migrate simultaneously into the framework with the fluoride ion.

Ultimately, the dominant resonances in the ^{19}F MAS NMR spectra of H–Y(F) and NH_4–Y(F) may be assigned to [SiO_3F] and [AlO_3F] moieties

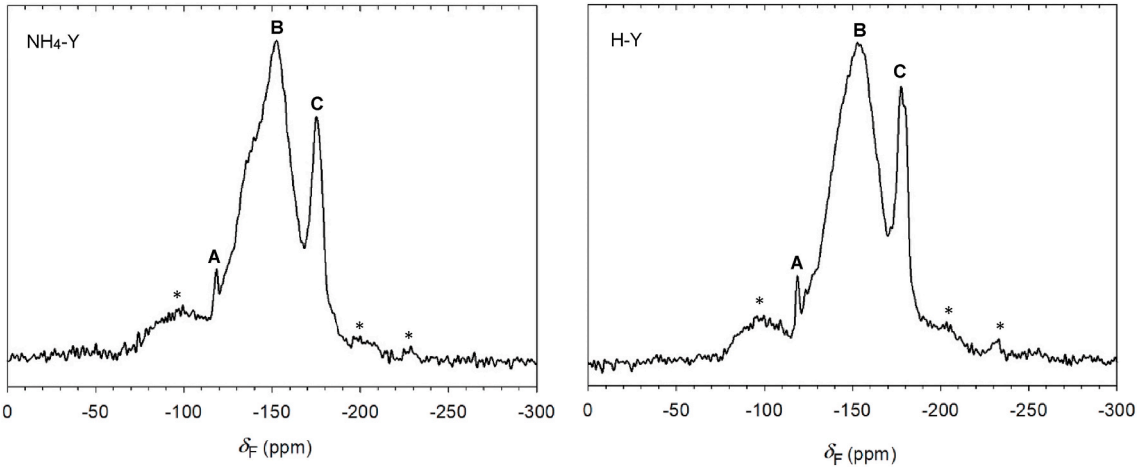

Fig. 5. ^{19}F MAS NMR spectra recorded on fluorinated NH_4–Y (left) and H–Y (right). * denotes spinning sidebands. Peaks are labelled A, B and C as discussed in the text.

in the zeolite. The presence of these moieties following fluorination further supports that fluoride interacts by "chemical adsorption", reacting with the zeolite framework, as indicated previously by adsorption energies derived from fitting to the DR isotherm. Indeed, the presence of these environments in NH_4–Y(F), fluorinated at 25 °C, confirms that chemisorption is occurring despite the lower than expected E_c value. It appears the presence of extra-framework aluminium-containing species within H–Y do not affect the interaction between the zeolite and fluoride, as the resonances present in the ^{19}F MAS NMR spectra are the same for both H–Y and NH_4–Y. ^{19}F MAS NMR also reveals the migration of small quantities of NaF ion-pairs into the zeolite, as evidenced by the resonance attributed to intrapore fluoride.

3.6. Fluorination mechanism

Assignments in the MAS NMR spectra of H–Y(F) and NH_4–Y(F) indicate that fluoride reacts with the zeolite framework to form $[SiO_3F]$ and $[AlO_3F]$ moieties. The acid-mediated fluorination of zeolite frameworks to produce these moieties may proceed by two plausible mechanisms, illustrated in Fig. 6. Mechanism 1 depicts the substitution of fluoride at surface hydroxyl groups (either silanol or aluminol) proceeding by the protonation of the hydroxyl group followed by the elimination of water, enabling fluoride to form a bond to silicon or aluminium. Alternatively, the addition of H^+F^- ion-pairs across T-O-T bonds could also lead to fluorination of the framework as illustrated in mechanism 2 in Fig. 6. Critically, mechanism 1 would lead to a commensurate decrease in surface hydroxyl moieties with increasing fluoride loading, whereas the reaction proceeding by mechanism 2 would lead to a corresponding increase in the surface hydroxyl concentration with increasing fluoride loading. This distinction may be exploited to determine which mechanism is occurring by measuring $^{29}Si\{^1H\}$ cross-polarised MAS NMR (CP MAS NMR) spectra on the fluorinated zeolites.

In the ^{29}Si MAS NMR spectra of zeolites, Q^3 Si(nAl) resonances typically appear at a chemical shift a few ppm downfield of the corresponding Q^4 Si(nAl) resonance. Consequently, Q^3 Si(n-1Al) resonances often appear co-incident with Q^4 Si(nAl) resonances in ^{29}Si MAS NMR spectra [34]. In $^{29}Si\{^1H\}$ CP MAS NMR, magnetisation is transferred from the ^1H nuclei of the silanol moieties to the ^{29}Si nuclei, enhancing the intensity of Q^3 Si resonances [34]. As all nominally assigned Q^4 Si (nAl) resonances, except Si(0Al), will have some Q^3 Si(n-1Al) contribution, comparing changes in peak intensity in the $^{29}Si\{^1H\}$ CP MAS NMR spectra between the parent material and fluorinated derivative may intimate by which mechanism the reaction proceeds.

Fig. 7 depicts the $^{29}Si\{^1H\}$ CP MAS NMR spectra of NH_4–Y and NH_4–Y(F), where intensity has been normalised such that the intensities

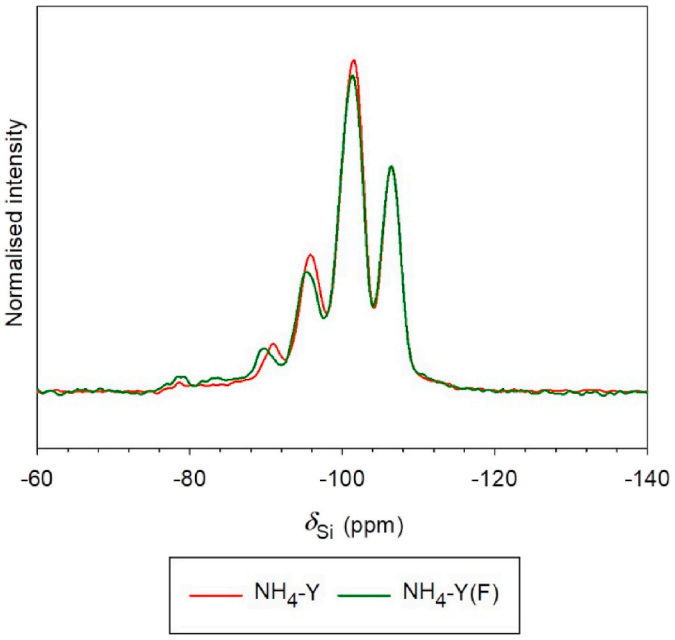

Fig. 7. Normalised $^{29}Si\{^1H\}$ CP MAS NMR spectra for NH_4–Y and NH_4–Y(F).

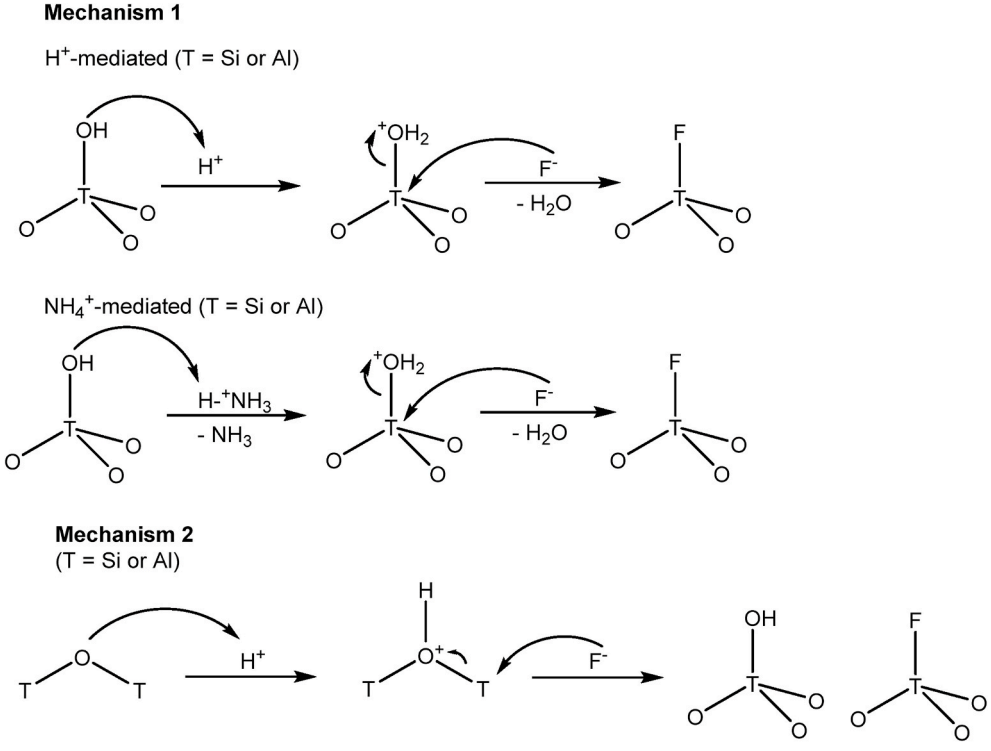

Fig. 6. Possible mechanisms for the fluorination of zeolite frameworks.

of the Si(0Al) peaks ($\delta_{Si} \approx -106$ ppm) are equivalent in both spectra to allow comparisons on differing intensities in the other peaks. In the spectra in Fig. 7, the Si(1Al), Si(2Al) and Si(3Al) peaks occur at $\delta_{Si} \approx -101$, −96 and – 90 ppm, respectively. A decrease in the intensity of the Si(1Al) and Si(2Al) peaks is apparent for NH_4–Y(F), compared with the parent material, NH_4–Y, indicating the silanol concentration decreases following fluorination, and therefore the reaction likely proceeds by mechanism 1, the substitution of fluoride at surface hydroxyl moieties. A downfield shift is observed in the Si(1Al), Si(2Al) and Si(3Al) peaks of NH_4–Y(F), compared with the peak positions in the NH_4–Y spectrum, with the magnitude of the shift increasing with increasing *n*. The origin of this shift is unclear but may relate to the different intrapore cation concentration in NH_4–Y(F), resulting from ion exchange between aqueous Na^+ and intrapore NH_4^+ during the treatment.

3.7. $M_x(NH_4)_{1-2x}$-Y: characterisation

The influence of intrapore cation on zeolite fluorination has been further studied for zeolite Y containing divalent intrapore cations, as divalent cations possess greater charge density than monovalent cations, and the presence of divalent cations within channels lowers the overall cation concentration thus increasing accessibility to guest species. NH_4–Y partially ion-exchanged with alkaline earth cations, $M_x(NH_4)_{1-2x}$-Y ($M = Mg^{2+}$, Ca^{2+}, Sr^{2+} or Ba^{2+}), have been characterised by PXRD and XRF spectrometry. PXRD patterns and unit cell parameters may be found in the Supporting Information. The extent of ion-exchange has been quantified by XRF spectrometry; Table 2 contains the Si/Al and M/Al ratios measured for $M_x(NH_4)_{1-2x}$-Y species, where *x* in the formula has been determined for each species directly from the M/Al ratio.

3.8. $M_x(NH_4)_{1-2x}$-Y: fluoride loadings and DR isotherms

Equilibrium fluoride loadings (q_e) attained across the concentration range (5–60 ppm F^-) at 25 °C for $M_x(NH_4)_{1-2x}$-Y species are plotted in Fig. 8, for comparison loadings measured for the parent material, NH_4–Y, are also plotted. The partial exchange of M^{2+} in all cases leads to enhanced equilibrium F^- loadings achieved by the zeolite across the entire concentration range. Analogous plots for equilibrium loadings at 40 °C (Supporting Information) demonstrate modest increases in loading upon increasing temperature.

Applying the linear DR equation to equilibrium uptake data for $M_x(NH_4)_{1-2x}$-Y species leads to good agreement in all instances, with $R^2 > 0.988$ for each species at both temperatures. DR plots at each temperature are presented in Fig. 9. R^2 values for fits along with E_c calculated for each plot are collated in Table 3. In each instance where a divalent cation has been partially exchanged into NH_4–Y, the characteristic fluoride adsorption energy is greater at 25 °C than the value for the parent material, NH_4–Y (7.5 kJ mol^{-1}). For each $M_x(NH_4)_{1-2x}$-Y species, increasing the temperature from 25 to 40 °C leads to a further increase in E_c. Modest increases are observed for $Ca_{0.17}(NH_4)_{0.66}$-Y and $Sr_{0.14}(NH_4)_{0.72}$-Y upon increasing the temperature to 40 °C (*ca.* 0.1–0.2 kJ mol^{-1}), whereas greater increases in E_c are observed upon increasing the temperature for $Mg_{0.15}(NH_4)_{0.70}$-Y and $Ba_{0.21}(NH_4)_{0.58}$-Y.

Table 2
M/Al and Si/Al measured for $M_x(NH_4)_{1-2x}$-Y by XRF spectrometry.

Zeolite	M/Al	Si/Al
NH_4–Y	–	2.7(1)
$Mg_{0.15}(NH_4)_{0.70}$-Y	0.15(1)	2.7(1)
$Ca_{0.17}(NH_4)_{0.66}$-Y	0.17(1)	2.7(1)
$Sr_{0.14}(NH_4)_{0.72}$-Y	0.14(1)	2.6(1)
$Ba_{0.21}(NH_4)_{0.58}$-Y	0.21(1)	2.6(1)

3.9. $M_x(NH_4)_{1-2x}$-Y: fluorine environment

Fluorine-19 MAS NMR spectra recorded for $M_x(NH_4)_{1-2x}$-Y species, treated with 60 ppm F^- NaF solutions for 24 h at 25 °C, are presented in Fig. 10. The approximate chemical shifts for resonances 1–4 (as labelled in Fig. 10) in each spectrum are listed in Table 4. The spectra recorded on NH_4–Y partially exchanged with alkaline earth metals (Mg, Ca, Sr and Ba) resemble the spectrum for the fluorinated parent material (NH_4–Y (F)): all contain the same 3 peaks at similar chemical shifts within the range −115 to −180 ppm with some spinning sidebands outside this range. The only significant difference is the appearance of an additional peak (**2**) at $\delta_F \approx -135$ ppm in the spectra for all $M_x(NH_4)_{1-2x}$-Y species. While there is no distinct maximum at $\delta_F \approx -135$ ppm in the $Ca_{0.17}(NH_4)_{0.66}$-Y(F) spectrum, peak fitting demonstrates there is a resonance at this chemical shift (Supporting Information). Peak fitting also indicates there is likely a resonance at $\delta_F \approx -135$ ppm in the fluorinated parent material, NH_4–Y(F); however, the estimated integral of this resonance in the NH_4–Y(F) spectrum is less than in spectra recorded on fluorinated $M_x(NH_4)_{1-2x}$-Y species.

Peak **1** in the ^{19}F MAS NMR spectra of fluorinated $M_x(NH_4)_{1-2x}$-Y species corresponds to peak **A** at $\delta_F \approx -119$ ppm in the NH_4–Y(F) spectrum and is therefore attributed to the intrapore fluoride environment. Peak **3** corresponds to the [SiO_3F] resonance which dominates the NH_4–Y(F) spectrum (peak **B**) at $\delta_F \approx -153$ ppm, however in the $M_x(NH_4)_{1-2x}$-Y spectra this resonance occurs at δ_F shifted downfield by 3–8 ppm. The higher chemical shift of the [SiO_3F] resonance reflects deshielding of the fluorine nuclei caused by the greater charge density of the divalent intrapore cations. Peak **4** corresponds to the [AlO_3F] resonance at $\delta_F \approx -176$ ppm in the NH_4–Y(F) spectrum (peak **C**); this resonance also occurs at δ_F shifted downfield by 3–8 ppm, for analogous reasons to peak **3**. The relative intensity of the [AlO_3F] peak appears to be reduced compared with the corresponding intensity in the NH_4–Y(F) spectrum; the origin of this diminished intensity is not clear.

The origin of peak **2** observed at $\delta_F \approx -135$ ppm in all spectra is unclear. The invariance of the chemical shift with different M^{2+} ions within the system, and the likely presence of this environment in NH_4–Y (F), indicates the environment is not directly bonded to the M^{2+} ion [35]. If present in $M_x(NH_4)_{1-2x}$-Y species, resonances for [SiO_4F] moieties would be expected at $\delta_F \approx -135$ ppm, approximately 10 ppm downfield of the [SiO_3F] resonances [5]; however, the ^{29}Si MAS NMR spectrum recorded on fluorinated $Sr_{0.14}(NH_4)_{0.72}$-Y, (Supporting Information), shows no intensity in the region where five co-ordinate silicon resonances would be expected ($\delta_{Si} \approx -145$ ppm) [5]. It could be argued that the proportion of silicon in five co-ordinate species would be too low to give rise to a discernible peak in the spectrum; however, if only 40% of the fluoride adsorbed to $Sr_{0.14}(NH_4)_{0.72}$-Y were bonded to silicon in [SiO_4F] moieties, this would correspond to *ca.* 1% of all silicon atoms within the zeolite being present as [SiO_4F] moieties. A discernible peak would therefore be expected if [SiO_4F] moieties were responsible for peak **2**; ultimately, it is unlikely these moieties are responsible for the unassigned resonance. Furthermore, there is no satisfactory explanation for how the [SiO_4F] moiety may be produced in the fluorinated zeolites by a proton-mediated process.

A resonance at $\delta_F \approx -135$ ppm has been observed in fluorinated derivatives previously, where the identity remained unsolved [15,16]. The [SiO_2F_2] moiety was put forward in each study as a candidate responsible for the resonance, but no evidence for this assignment was provided. For fluorination to proceed by the proposed mechanism, [SiO_2F_2] could only be produced by substitution of fluoride for both hydroxide components of geminal silanol moieties (i.e. [$SiO_2(OH)_2$]).

A new theoretical explanation for the unassigned resonance is that it is caused by neighboring or proximal [SiO_3F] groups. The presence of [SiO_3F] groups in close proximity could cause deshielding of the fluorine nuclei and a consequent downfield shift in δ_F from the values typically associated with [SiO_3F] resonances. If sufficiently close, fluoride atoms bonded to the framework could exert Coulombic repulsion on one

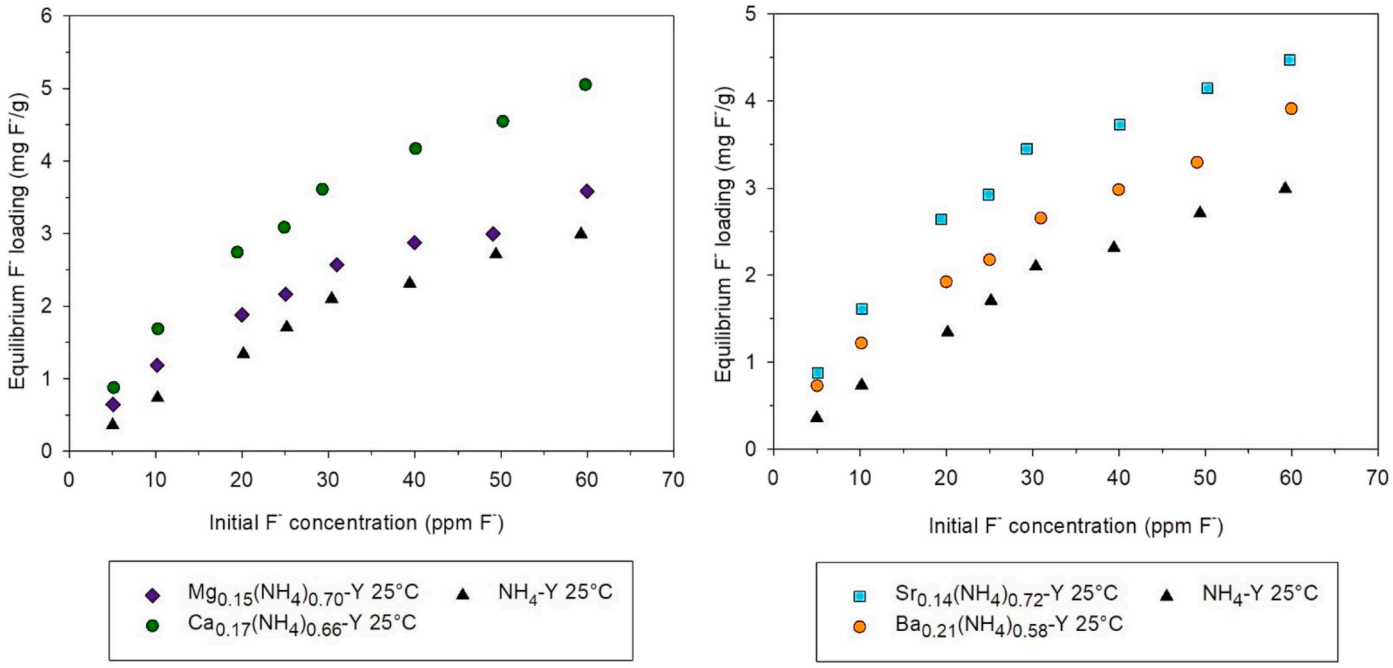

Fig. 8. Equilibrium fluoride loadings achieved at 25 °C by $Mg_{0.15}(NH_4)_{0.70}$-Y and $Ca_{0.17}(NH_4)_{0.66}$-Y (left), and $Sr_{0.14}(NH_4)_{0.72}$-Y and $Ba_{0.21}(NH_4)_{0.58}$-Y (right).

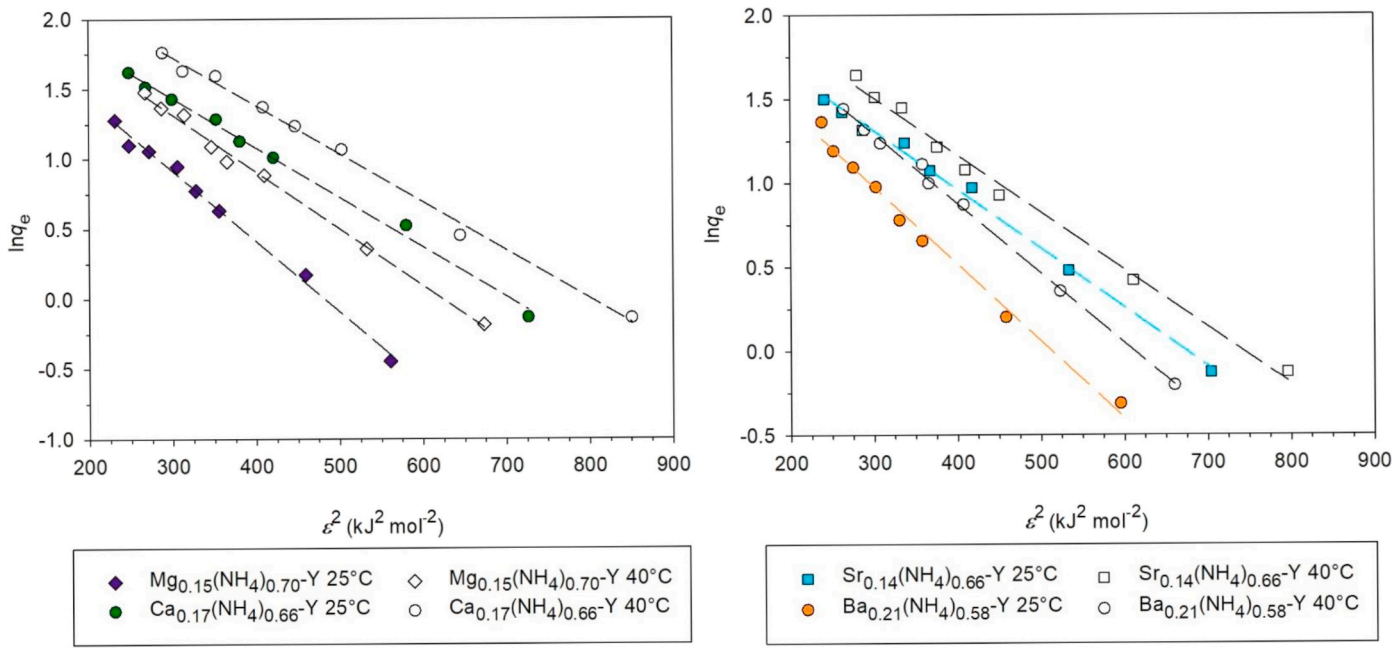

Fig. 9. DR plots for $Mg_{0.15}(NH_4)_{0.70}$-Y and $Ca_{0.17}(NH_4)_{0.66}$-Y (left), and $Sr_{0.14}(NH_4)_{0.72}$-Y and $Ba_{0.21}(NH_4)_{0.58}$-Y (right).

Table 3
R^2 and E_c for fits to the linear DR equation for $M_x(NH_4)_{1-2x}$-Y.

Zeolite	T (°C)	R^2	E_c (kJ mol^{-1})
$Mg_{0.15}(NH_4)_{0.70}$-Y	25	0.993	10.0
	40	0.995	11.1
$Ca_{0.17}(NH_4)_{0.66}$-Y	25	0.995	11.9
	40	0.995	12.0
$Sr_{0.14}(NH_4)_{0.72}$-Y	25	0.994	11.9
	40	0.992	12.1
$Ba_{0.21}(NH_4)_{0.58}$-Y	25	0.989	10.4
	40	0.997	11.0

another through space, serving to distort the electron cloud and subsequently affect the shielding of the fluorine nuclei. Furthermore, the presence of fluorine substituents on neighboring silicon atoms in the framework could lead to increased polarity of the Si–F bonds, deshielding the fluorine nuclei through inductive effects. Comparable downfield shifts (*ca.* 10 ppm) are observed in ^{19}F NMR spectra upon the introduction of fluorine substituents at neighboring carbon atoms in fluoroalkanes [37].

If proximal [SiO_3F] groups are responsible for the resonance, the question of how the divalent cations promote reactivity at proximal silanol groups is raised. It is surmised that a divalent cation on the zeolite surface co-ordinates the fluoride ion prior to the reaction,

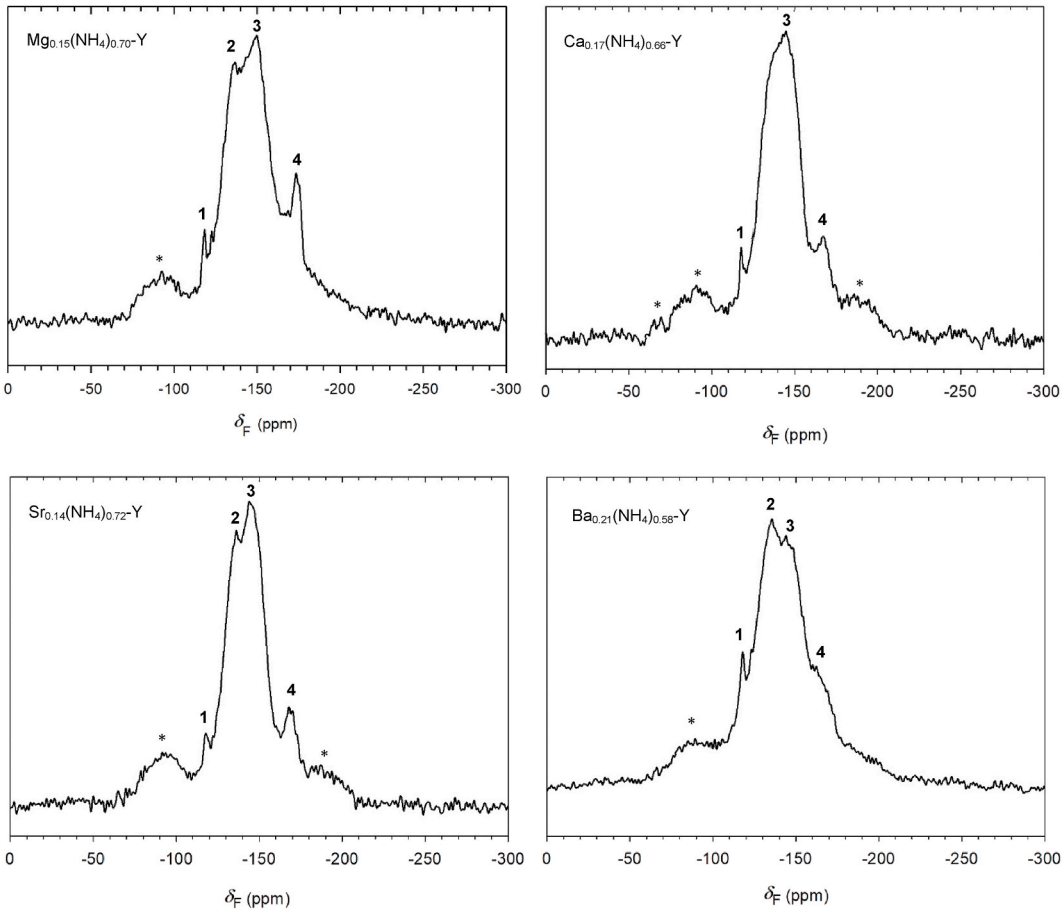

Fig. 10. ^{19}F MAS NMR spectra of fluorinated $M_x(NH_4)_{1-2x}$-Y species as labelled. * denotes spinning sidebands. Peaks are labelled 1–4 as discussed in the text.

Table 4
Approximate chemical shifts in ^{19}F MAS NMR spectra for $M_x(NH_4)_{1-2x}$-Y species and NH_4–Y.

Zeolite	δ_F (ppm)			
	1	2	3	4
NH_4–Y	−119		−153	−176
$Mg_{0.15}(NH_4)_{0.70}$-Y	−118	−137	−150	−174
$Ca_{0.17}(NH_4)_{0.66}$-Y	−118	−134	−145	−167
$Sr_{0.14}(NH_4)_{0.72}$-Y	−118	−136	−144	−168
$Ba_{0.21}(NH_4)_{0.58}$-Y	−118	−136	−144	−166

bringing the fluoride into close proximity to silanol moieties that may neighbor the divalent cation, allowing a reactive intermediate to form more readily. A divalent cation in a fixed position on the surface could promote the reaction on two or more proximal silanol groups if they are present, whereas in the absence of a divalent cation, reactivity at silanol groups is expected to be random. Moreover, in the absence of divalent cations, the Coulombic repulsion incurred by proximal fluoride ions may prevent the formation of proximal [SiO_3F] moieties in any significant concentration. Naturally, the proximal [SiO_3F] assignment, and how divalent cations may promote reactivity at proximal silanol groups, remains only a theory unless empirically proven.

Except for the unassigned peak at $\delta_F \approx -135$ ppm, which may also be present in NH_4–Y(F), the fluorine environments observed in fluorinated $M_x(NH_4)_{1-2x}$-Y species correspond to those observed in NH_4–Y(F), containing [SiO_3F], [AlO_3F] and intrapore fluoride. Critically, while higher fluoride loadings and increased characteristic adsorption energies are observed for $M_x(NH_4)_{1-2x}$-Y species, there is no evidence that the divalent cations directly co-ordinate the fluoride ions. It would appear the divalent cations promote the fluorination of zeolites without directly coordinating the fluoride ions. A full understanding of how divalent cations promote the reaction is hindered by the unassigned resonance in the ^{19}F MAS NMR spectra of the fluorinated zeolites.

It was reported in a study on defluoridation by a natural Ca/Na-STI sample that ion-exchange between intrapore Ca^{2+} and aqueous Na^+ followed by precipitation of CaF_2 was responsible for observed fluoride uptake [10]. ^{19}F MAS NMR spectra recorded on alkaline-earth exchanged zeolites ($M_x(NH_4)_{1-2x}$-Y) contain no resonance corresponding to MF_2 species, which would be expected at −107 (CaF_2), −83.2 (SrF_2), −196 (MgF_2) and −11.2 ppm (BaF_2), respectively [35]. All MF_2 species for M containing zeolites, except CaF_2, have a greater solubility than the highest fluoride concentration employed in these studies, as a result ion-exchange between aqueous Na^+ and intrapore M^{2+} could not give rise to MF_2 precipitation in these systems [36]. In the case of CaF_2, precipitation could occur from solutions with concentrations greater than 7 ppm F^-, provided a stoichiometric equivalence of Ca^{2+} were present in solution. The absence of a resonance at $\delta_F \approx -107$ ppm in the ^{19}F MAS NMR spectrum of $Ca_{0.17}(NH_4)_{0.66}$-Y(F) confutes the calcium fluoride precipitation theory.

3.10. M_xNa_{1-2x}-Y: fluoride loadings

M_xNa_{1-2x}-Y (M = Mg^{2+}, Ca^{2+}, Sr^{2+} or Ba^{2+}) prepared by ion-exchange, analogously to $M_x(NH_4)_{1-2x}$-Y, have been characterised by PXRD and XRF spectrometry (Supporting Information). Equilibrium fluoride loadings (q_e) for M_xNa_{1-2x}-Y and $M_x(NH_4)_{1-2x}$-Y from 20 ppm F^- solutions at 25 °C are listed in Table 5. Despite higher divalent metal content in M_xNa_{1-2x}-Y compared with $M_x(NH_4)_{1-2x}$-Y, equilibrium loadings for M_xNa_{1-2x}-Y are much lower than the analogous $M_x(NH_4)_{1-}$

Table 5
Equilibrium fluoride loadings achieved by M_xNa_{1-2x}-Y and $M_x(NH_4)_{1-2x}$-Y from 20 ppm F^- NaF solutions at 25 °C.

M	q_e, M_xNa_{1-2x}-Y (mg g^{-1})	q_e, $M_x(NH_4)_{1-2x}$-Y (mg g^{-1})	% (q_e, M_xNa_{1-2x}-Y)/(q_e, $M_x(NH_4)_{1-2x}$-Y)
Mg	0.11	1.88	5.9
Ca	0.14	2.74	5.1
Sr	0.07	2.64	2.6
Ba	0.12	1.92	6.3

$_{2x}$-Y species with equilibrium loadings for M_xNa_{1-2x}-Y corresponding to between 2.6 and 6.3% of the loadings attained for $M_x(NH_4)_{1-2x}$-Y. As the pH of the solutions are near neutral (pH = 6.8) and there is no proton source, this further supports the essential role of a proton source in mediating fluoride uptake in the divalent substituted zeolites.

While the fluoride loadings achieved for M_xNa_{1-2x}-Y species are low compared with the loadings for $M_x(NH_4)_{1-2x}$-Y under the same conditions, there is still detectable fluoride uptake for M_xNa_{1-2x}-Y which is not observed for the parent compound Na–Y under the same conditions. As there is no H^+ source, the only fluoride environment observed in $M_x(NH_4)_{1-2x}$-Y species that would be anticipated in the Na analogues is the intrapore fluoride environment. The presence of this environment in M_xNa_{1-2x}-Y but not in Na–Y may be rationalised by the greater accessibility to the pores afforded by lower intrapore cation concentrations, allowing the migration of Na^+F^- ion pairs into the framework. Intrapore fluoride ions being responsible for the observed uptake in M_xNa_{1-2x}-Y remains supposition, however, as NMR experiments have not been performed on fluorinated M_xNa_{1-2x}-Y species to confirm this assignment, due to the low fluoride content and long experiment durations required to obtain informative spectra.

4. Conclusions

NH_4–Y and H–Y exhibit reactivity with aqueous fluoride, whereas Na–Y does not. The importance of a H^+ source in mediating the fluorination reaction between the zeolite and fluoride has been established. Moreover, by employing ^{19}F MAS NMR spectroscopy to probe the local environment, it has been determined that fluoride reacts with the framework forming four co-ordinate fluorine containing species, [SiO_3F] and [AlO_3F]. A minor amount of fluoride is also present as fluoride ions in the pores, suggesting the migration of some Na^+F^- ion-pairs into the zeolite. $^{29}Si\{^1H\}$ CP MAS NMR spectra have been used to differentiate between two plausible mechanisms for the fluorination reaction in NH_4–Y, intimating the reaction proceeds by substitution of fluoride at surface hydroxyl groups, the same mechanism by which fluorination is reported to proceed in hydrothermal and high temperature treatments on other zeolites, as inferred in those reports by IR spectroscopy [15,21].

Findings on the fluorination of zeolite frameworks have important implications on the potential application of zeolites in defluoridation, as the environmental remediation of excess aqueous fluoride from solutions with typical concentrations 20–50 ppm fluoride is desirable [8,14]. Here, the efficacy of H^+ and NH_4^+-bearing zeolite Y in fluoride uptake from solutions in this concentration range has been demonstrated. In addition, the fluorination of zeolites under mild conditions, 25 °C and 200 ppm fluoride solutions, has achieved significant loadings (*ca.* 2 wt %) for zeolites containing acidic intrapore cations. These conditions achieve loadings comparable with those reported for fluorinated zeolites prepared for catalytic applications [18], yet under significantly milder and safer conditions.

Partial ion-exchange of alkaline earth divalent cations (Mg^{2+}, Ca^{2+}, Sr^{2+} and Ba^{2+}) into NH_4–Y leads to enhanced fluoride loadings achieved and an increase in the characteristic adsorption energy in all cases, compared with the parent material (NH_4–Y). In contrast, there is little change in the fluoride uptake measured for the divalent cation exchanged forms of Na–Y compared with the parent material, with comparatively low uptake observed for all M_xNa_{1-2x}-Y species. ^{19}F MAS NMR spectroscopy reveals no direct M-F bonds are formed in fluorinated $M_x(NH_4)_{1-2x}$-Y species, nor are MF_2 species precipitated, rather the reaction appears to proceed in the same manner as for NH_4–Y evidenced by resonances attributable to [SiO_3F], [AlO_3F] and intrapore fluoride species. An additional resonance of unknown origin is present at $\delta_F \approx -135$ ppm in the ^{19}F MAS NMR spectra; it has been postulated that the resonance is caused by proximal [SiO_3F] moieties with a downfield shift in δ_F caused by, either or both, through space Coulombic repulsion between near fluorine atoms and inductive effects leading to deshielding of the fluorine nuclei. A theory has been put forward for how M^{2+} cations could promote fluoride reactivity at adjacent silanol moieties; however, the assignment remains unproven. Ultimately, it appears the H^+-mediated mechanism for fluorination is also responsible for the observed uptake in $M_x(NH_4)_{1-2x}$-Y species. While there is no evidence to suggest that the divalent metal ion directly co-ordinates fluoride, the presence of divalent intrapore cations nevertheless increase the observed fluoride loadings and characteristic adsorption energies, therefore promoting reactivity between fluoride and the zeolite framework.

Declaration of competing interest

The authors declare that they have no known competing financial interests or personal relationships that could have appeared to influence the work reported in this paper.

Acknowledgements

This work was supported by the Schools of Chemistry and Chemical Engineering at the University of Birmingham.

Appendix A. Supplementary data

Supplementary data to this article can be found online at https://doi.org/10.1016/j.micromeso.2020.110470.

References

[1] A. Corma, M.J. Diaz-Cabanas, F. Rey, Chem. Commun. (2003) 1050–1051, https://doi.org/10.1039/b212477g.
[2] M. Estermann, L.B. McCusker, C. Baerlocher, A. Merrouche, H. Kessler, Nature 352 (1991) 320–323, https://doi.org/10.1038/352320a0.
[3] M. Hernandez-Rodriguez, J.L. Jorda, F. Rey, A. Corma, J. Am. Chem. Soc. 134 (2012) 13232–13235, https://doi.org/10.1021/ja306013k.
[4] P.A. Barrett, M. Camblor, A. Corma, R.H. Jones, L.A. Villaescusa, J. Phys. Chem. B 102 (1998) 4147–4155, https://doi.org/10.1021/jp980735e.
[5] H. Koller, A. Wölker, H. Eckert, C. Panz, P. Behrens, Angew. Chem. Int. Ed. 36 (1997) 2823–2825, https://doi.org/10.1002/anie.199728231.
[6] M.A. Camblor, M.J. Diaz-Cabanas, J. Perez-Pariente, S.J. Teat, W. Clegg, I. J. Shannon, P. Lightfoot, P.A. Wright, R.E. Morris, Angew. Chem. Int. Ed. 37 (1998) 2122–2126, https://doi.org/10.1002/(SICI)1521-3773(19980817)37:15<2122::AID-ANIE2122>3.0.CO, 2-6.
[7] H. Koller, A. Woelker, L.A. Villaescusa, M.J. Diaz-Cabanas, S. Valencia, M. A. Camblor, J. A. Chem. Soc. 121 (1999) 3368–3376, https://doi.org/10.1021/ja9840549.
[8] M. Adem, T. Sani, Y. Chebude, G. Fetter, P. Bosch, I. Diaz, Bull. Chem. Soc. Ethiop. 29 (2015) 53–62, https://doi.org/10.4314/bcse.v29i1.5.
[9] M. Maruthamuthu, A. Sivasamy, Fluoride 27 (1994) 81–88.
[10] L.G. Hortiguela, A.B. Pinar, J. Perez-Pariente, T. Sani, Y. Chebude, I. Diaz, Microporous Mesoporous Mater. 193 (2014) 93–102, https://doi.org/10.1016/j.micromeso.2014.03.014.
[11] Y. Sun, Q. Fang, J. Dong, X. Cheng, J. Xu, Desalination 277 (2011) 121–127, https://doi.org/10.1016/j.desal.2011.04.013.
[12] M.S. Onyango, Y. Kojima, A. Kumar, D. Kuchar, M. Kubota, H. Matsuda, Separ. Sci. Technol. 41 (2006) 683–704, https://doi.org/10.1080/01496390500527019.
[13] S. Samatya, U. Yuksel, M. Yuksel, N. Kabay, Separ. Sci. Technol. 42 (2007) 2033–2047, https://doi.org/10.1080/01496390701310421.
[14] M.S. Onyango, Y. Kojima, O. Aoyi, E.C. Bernardo, H. Matsuda, J. Colloid Interface Sci. 279 (2004) 341–350, https://doi.org/10.1016/j.jcis.2004.06.038.
[15] X. Fang, Q. Wang, A. Zheng, Y. Liu, Y. Wang, X. Deng, H. Wu, F. Deng, M. He, P. Wu, Catal. Sci. Technol. 2 (2012) 2433–2435, https://doi.org/10.1039/c2cy20446k.

[16] X. Fang, Q. Wang, A. Zheng, Y. Liu, L. Lin, H. Wu, F. Deng, M. He, P. Wu, Phys. Chem. Chem. Phys. 15 (2013) 4930–4938, https://doi.org/10.1039/c3cp44700f.
[17] Y. Yang, J. Ding, B. Wang, J. Wu, C. Zhao, G. Gao, P. Wu, J. Catal. 320 (2014) 160–169, https://doi.org/10.1016/j.jcat.2014.10.008.
[18] X. Lu, W. Zhou, Y. Guan, A. Liebens, P. Wu, Catal. Sci. Technol. 7 (2017) 2624–2631, https://doi.org/10.1039/c7cy00428a.
[19] H.M. Kao, Y. Liao, J. Phys. Chem. C 111 (2007) 4495–4498, https://doi.org/10.1021/jp070739w.
[20] R. Le Van Mao, T.S. Le, M. Fairbairn, A. Muntasar, S. Xiao, G. Denes, Appl. Catal., A 185 (1999) 41–52, https://doi.org/10.1016/S0926-860X(99)00132-5.
[21] S. Kowalak, E. Szymkowiak, M. Laniecki, J. Fluor. Chem. 93 (1999) 175–180, https://doi.org/10.1016/S0022-1139(98)00312-1.
[22] D.S. Parsons, A. Ingram, J.A. Hriljac, MRS Adv 4 (2019) 21–26, https://doi.org/10.1557/adv.2018.635.
[23] K.Y. Foo, B.H. Hameed, Chem. Eng. J. 156 (2010) 2–10, https://doi.org/10.1016/j.cej.2009.09.013.
[24] Q. Hu, Z. Zhang, J. Mol. Liq. 277 (2019) 646–648, https://doi.org/10.1016/j.molliq.2019.01.005.
[25] J.G. Reynolds, J.D. Belsher, J. Chem. Eng. Data 62 (2017) 1743–1748, https://doi.org/10.1021/acs.jced.7b00089.
[26] J. Laugier, B. Bochu, LMGP Suite of Programs, Laboratoire des Matériaux et du Génie Physique, France, 2002.
[27] Y. Hong, J.J. Fripiat, Microporous Mater. 4 (1995) 323–334, https://doi.org/10.1016/0927-6513(95)00038-B.
[28] A. Bolshakov, N. Kosinov, D.E. Romero Hidalgo, B. Mezari, A.J.F. van Hoof, E.J. M. Hensen, Catal. Sci. Technol. 9 (2019) 4239–4247, 10.1039/C9CY00593E.
[29] I. Ogino, M. Nigra, S. Hwang, J. Ha, T. Rea, S.I. Zones, A. Katz, J. Am. Chem. Soc. 133 (2011) 3288–3291, https://doi.org/10.1021/ja111147z.
[30] R.E. Youngman, S. Sen, J. Non-Cryst. Solids 349 (2004) 10–15, https://doi.org/10.1016/j.jnoncrysol.2004.03.122.
[31] L. Delmotte, M. Soulard, F. Guth, A. Seive, A. Lopez, T.L. Guth, Zeolites 10 (1990) 778–783, https://doi.org/10.1016/0144-2449(90)90061-U.
[32] G. Zhang, B. Wang, W. Zhang, M. Li, Z. Tian, Dalton Trans. 45 (2016) 6634–6640, https://doi.org/10.1039/c6dt00424e.
[33] E.Y. Chekmenev, S.K. Chow, D. Tofan, D.P. Weitekamp, B.D. Ross, P. Bhattacharya, J. Phys. Chem. B 112 (2008) 6285–6287, https://doi.org/10.1021/jp800646k.
[34] G. Engelhardt, U. Lohse, A. Samoson, M. Magi, M. Tarmak, E. Lippmaa, Zeolites 2 (1982) 59–62, https://doi.org/10.1016/S0144-2449(82)80042-0.
[35] A. Zheng, S. Liu, F. Deng, J. Phys. Chem. C 113 (2009) 15018–15023, https://doi.org/10.1021/jp904454t.
[36] D.R. Lide (Ed.), CRC Handbook of Chemistry and Physics, 73rd ed, CRC Press, Boca Raton, FL, 1973.
[37] H.P. Ebrahimi, M. Tofazzoli, Concepts Magn. Reson. 40 (2012) 192–204, https://doi.org/10.1002/cmr.a.21238.